Arabian Journal of Geosciences (2022) 15: 1147
https://doi.org/10.1007/s12517-022-10419-5

ORIGINAL PAPER

Reservoir Evaluation of the Tertiary Succession in Selected Wells at Ajeel Oilfield, Northern Mesopotamian Basin, NE Iraq

Abbas F. Gharib[1,2] · **Ali Müjdat Özkan**[3]

Received: 27 February 2020 / Accepted: 1 June 2022 / Published online: 10 June 2022

Abstract

In the present study, a total of forty-five rock samples, well-logs data, and 3 crude-oil samples from reservoirs rocks, in addition to 70 rock samples from Jurassic–Cretaceous source rocks, are used to assess the Tertiary succession in the Ajeel oilfield. Examined thin sections prepared from core rock samples collected from several wells within the Ajeel oilfield indicated the presence of several microfacies in which different types of porosity such as intraparticle, interparticle, moldic, and vugs have been detected. Moreover, different diagenetic features, including cementation, dolomitization, recrystallization, dissolution, and microfractures, indicate that the examined formations were deposited in a marine depositional environment. Cross-plots of several well-logging data showed that Tertiary reservoir rocks can be divided into eight reservoir units composed predominantly of limestone, dolomitic limestone, and thin beds of anhydrite beds. In the majority of wells, these units had a total and effective porosity of up to 32.0% and 30%, respectively. A wide range of variation is observed in water saturation with the lowest being 5% and higher hydrocarbon contents, indicating that these formations are the main reservoirs in the Mesopotamian Basin. The geochemical investigation of crude-oils recognized paraffinic (medium-light), and sour crude-oils, which are originated mainly from marine-origin organic matters. Palynofacies examination showed that source rocks in the Mesopotamian Basin deposited mainly in distal suboxic-anoxic and distal dysoxic-oxic conditions with kerogen Type II (oil-prone), indicating that Jurassic–Cretaceous succession represents main sources rocks in northern Iraq.

Keywords Reservoir evaluation · Ajeel oilfield · Hydrocarbon-bearing zones · Tertiary succession · Jurassic–Cretaceous succession · Paraffinic crude-oils

Introduction

This research examines Iraq's oil-and-gas-producing Tigris subzone, which is situated in the Mesopotamian Basin's northern Tikrit governorate. Iraq is the Middle East's hydrocarbon-richest country and an OPEC leader, with proven oil reserves of up to 133 billion barrels and natural gas reserves of up to 110 trillion cubic feet (Horn 2003, 2004; Verma et al. 2004). It contains multiple petroleum systems spanning the Paleozoic, Mesozoic, and Cenozoic eras, making it one of the Middle East's largest producers of hydrocarbons, with the major oilfields situated within Mesopotamian–Zagros basins (Ahlbrandt et al. 2000; Pitman et al. 2004; Verma et al. 2004).

The Mesopotamian Basin, which encompasses Iraq, Kuwait, and Iran, is one of the world's most significant hydrocarbon basins (Fig. 1). Petroleum exploration in this Basin is started by Iraqi Oil Companies (IOC) approximately in late 1920. It contains many important oilfields, such as Majnoon, West Qurna, Nah Umr, Rumaila, Subba, Ratawi, Zubair, Balad, East Baghdad, Ajeel, and Tikrit Oilfields (Fig. 1), and this Basin has attracted the attention of academic researchers and the oil and gas industry due to its potential for conventional petroleum investigations and development (Altameemi and Alzaidy 2018; Mamaseni et al. 2018; Hamdullaa et al. 2018; Abeed et al. 2019; Al-Khafaji et al. 2021; Gharib et al.

Responsible Editor: Narasimman Sundararajan

✉ Abbas F. Gharib
abass.falah@sadiq.edu.iq; abbas_falah1987720@yahoo.com

1 Department of Oil and Gas Economics, College of Administrative and Financial Science, Imam Ja'afar Al-Sadiq University, Baghdad, Iraq

2 Geological Engineering Department, Selçuk University, Selçuklu, Konya, Turkey

3 Geological Engineering Department, Konya Technical University, 42250 S Konya, Turkey

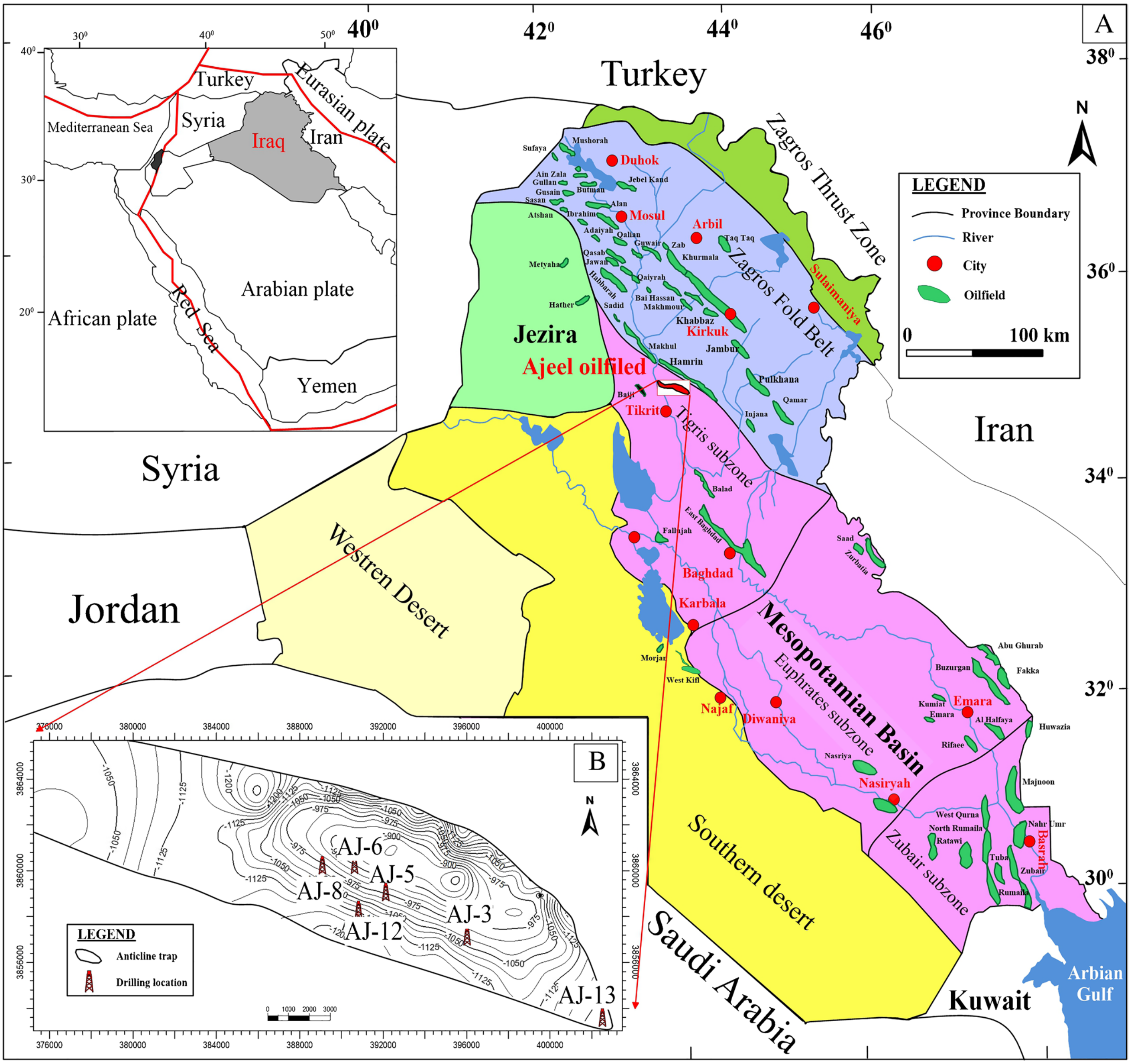

Fig. 1 **A** Location map of studied area **B** Structural contour map and well locations

2021). Previous studies have evaluated the reservoir characterization and sedimentology of the cretaceous formations in central and southern Iraq (e.g., Al-Fandi et al. 2020; Altameemi and Alzaidy 2018; Mamaseni et al. 2018; Mohammed et al. 2021, 2022). Stratigraphic correlation and depositional setting of Miocene Euphrates and Jeribe formations in northern and southern Iraq have been studied by Ctyrokey and Karim (1971); Hussein et al. (2017); Ahmed et al. (2021); and Abdullah et al. (2019). However, no detailed reservoir characteristics investigations have been undertaken within a well-logging and geochemical context of the Ajeel oilfield (discovered in the 1970s) which prompted the present research.

The study area is presented by Ajeel oilfield in the northwestern part of the Mesopotamian Basin, NE Iraq (Fig. 1), containing communicating carbonate reservoirs with primary production from the carbonate units of the Tertiary Serikagni, Euphrates, Dhiban, and Jeribe formations (Fig. 2), while Jurassic and Cretaceous organic-rich marine carbonate and shale successions including Sargelu, Naokelekan/Najmah, Gotnia, and Chia Gara formations are the main sources of hydrocarbons in the Iraqi petroleum region (Alsharhan and Nairn 1997; Pitman et al. 2004; Al-Ameri and Zumberge 2013; Badics and Aqrawi 2015). Therefore, this study tries to find genetic links between Tertiary reservoir rocks and

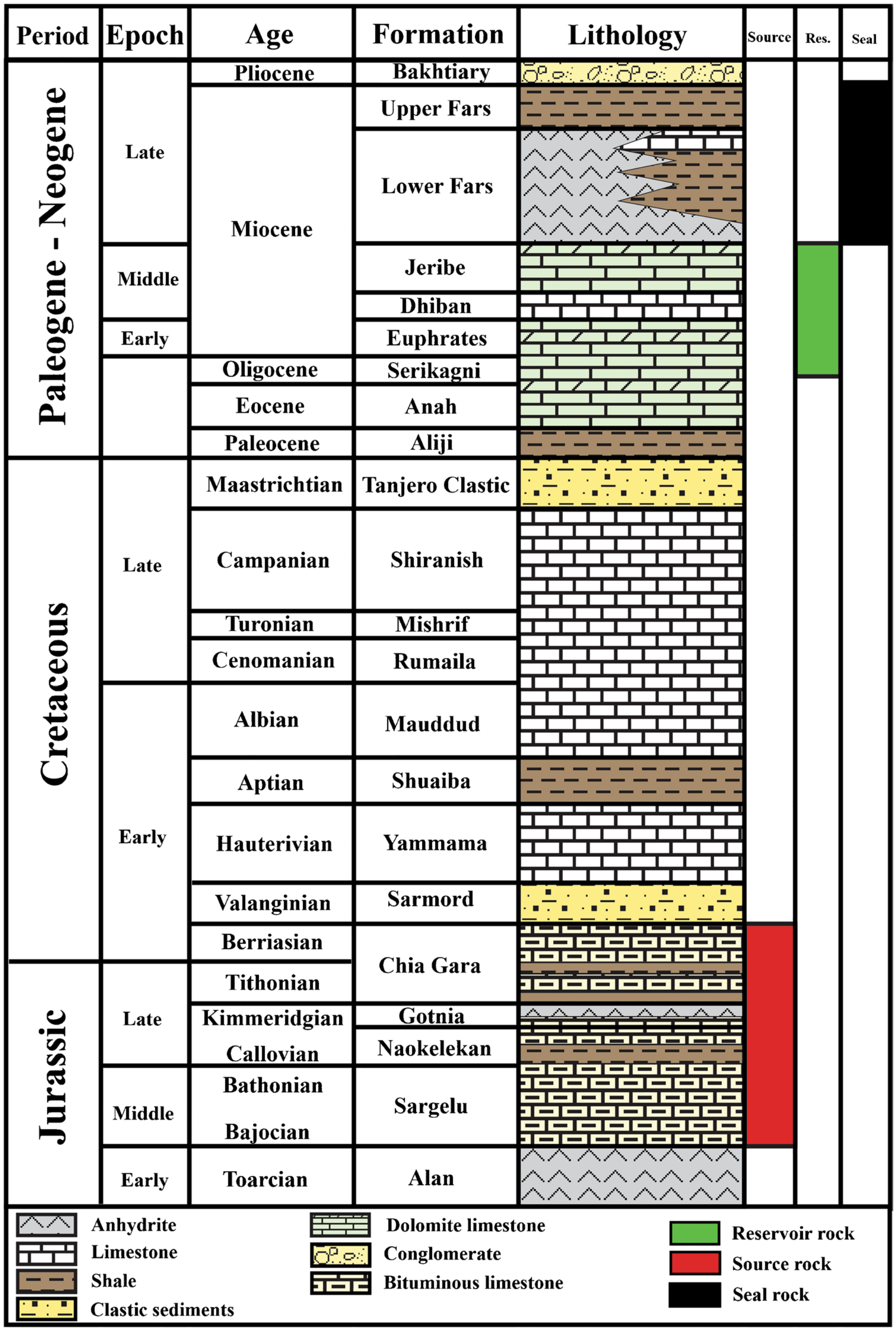

Fig. 2 The stratigraphic columnar shows lithostratigraphic units of the Ajeel oilfield

source rocks in producing Ajeel field. In this regard, there are a total of 45 rock samples, well-logging data of four wells, and three crude-oils from Tertiary reservoir rocks, as well as 70 core and cutting samples, from Jurassic–Cretaceous succession.

The current study aims to determine (1) the lithology, depositional environment, diagenesis, porosity types identification, (2) total (PHIT) and secondary porosity (PHIE) estimation, (3) shale content (V_{CL}) measurements, (4) water saturation (S_W), and bulk volume of water (B_{VW}, $B_{VW}S_{XO}$) determination, (5) crude-oil characterization, and (6) palynological evaluation in order to conclude the depositional environment and predict hydrocarbon-generation potential of these formations in the Mesopotamian Basin, NE Iraq.

Geological background

Iraq is sandwiched among the Iranian–Turkish and Arabian Plates (Fig. 1a), with the N-NE edges restricted by the Taurus and Zagros sutures, and the NW-SW edge is bounded by the Dead and the Red Seas, respectively (Beydoun 1991; Sadooni and Aqrawi 2000). Ajeel oilfield is situated inside the Tigris subzone, about 35 km north of Tikrit governorate at the northwest margin of the Mesopotamian, NE Iraq, with a symmetrical anticline of the NW–SE trending axis (Fig. 1). The anticlinal structures in Iraq are formed as a result of multiple stages of convergence of thin-skinned sediments and Paleozoic age basements. The Mesopotamian Basin is one of the most important petroleum provinces that extends from northwest to southeast Iraq with several discovered hydrocarbon fields (Buday 1980a; Jassim and Goff 2006; Al-Khafaji et al. 2018, 2019, 2021). The Mesopotamian Basin is about 800 km across and subdivided from north to south into the Tigris, Euphrates, and Zubair subzones.

Iraq's Oligocene–Pliocene age is divided into two sedimentological cycles, (1) the Oligocene–Middle Miocene succession which includes Ghar, Serikagni, Euphrates Limestone, Dhiban Anhydrite with minor amounts of limestone beds, Jeribe Limestone, and Injanah formations; (2) the Upper Miocene–Pliocene succession, which includes the Zahra, Dibdibba, Fatha, and Bakhtiari formations (Buday 1980b).

The Arabian Plate can be divided into the Arabian Shield and the Arabian Shelf. The Arabian shelf in Iraq can be divided into a stable shelf and an unstable shelf (Jassim and Buday 2006). They consist of five tectono-physiographic zones that are generally bounded by major faults that may represent deep-seated structural elements. These tectonic zones include (1) the thrust zone, (2) the folded zone, (3) the Mesopotamian Basin, (4) the Salman zone, and (5) the Rutbah-Jezira zone (Ameen 1992; Jassim and Goff 2006). The Cretaceous and Tertiary oil habitat of the supergiant oilfields in northern Iraq is a result of several geological processes that started during the Middle-Upper Triassic time when the Neo-Tethys Ocean began to form at the expense of the Paleo-Tethys farther north. During this period, the central part of Iraq and the Mesopotamian Zone has received considerably thicker sedimentation that reached 4500 m. Later during the Jurassic–Early Cretaceous periods, the carbonate source rocks are deposited as a result of major inundation and the spotted constructional high during Kimmeridgian-Tithonian resulted in restriction and isolation from the open marine of the Neo-Tethys. The Cretaceous and the Paleocene Periods represent the pre-collisional stage which involved deposition on the marginal cratonic platform, quasi-platform, and the foreland basin of the passive continental margin of the Arabian Plate; and on the active continental margins and island arcs of the Iranian and Turkish Plates. Finally, Neo-Tethys are closed during the Eocene period, and the Arabian plate collided with the active margins of the Iranian and Turkish Plates. However, the tectonic movement of the Arabian and Eurasian plates produced Jurassic–Cretaceous-to-late-Paleogene–Neogene successions of both marine and non-marine sediments, interrupted by numerous periods of erosional events and unconformities (Ameen 1992; Al-Khafaji et al. 2018).

Figure 1 depicts the general lithology of the Ajeel oilfield. The Serikagni, Euphrates, Dhiban, and Jeribe reservoir rocks, as well as Fatha, Injana cap rocks, and Bakhtiari conglomerates, are predominantly Tertiary rocks.

The Serikagni formation (Fig. 2), initially reported by Bellen in 1955 in the Jebel Sinjar region, is overlain directly by the Euphrates formation and underlined by Anah formation (Buday 1980b; Jassim and Goff 2006). Furthermore, this formation contains *Globigerina*, chalky limestone with a few off-shore calcareous sediments (Al-Dabbas and Hassan 2013; Koyi and Mansurbeg 2021).

The Euphrates formation as described by De Boeckh in 1929 near Wadi Fuhaimi (Bellen et al. 1959; Ahmed et al. 2021) comprises of recrystallized limestone, dolomite, dolomitic limestone, and shelly limestone beds. The Dhiban formation is conformably overlain by the Jeribe formation (Fig. 2), it is described by Henson in 1940 inthe Sinjar area, Foothill Zone comprises of anhydrite, interbedded dolomite, and limestone layers.

Bellen first is introduced the Jeribe formation in 1957 at Sinjar anticline (Bellen et al. 1959; Lawa et al. 2020), it comprises of recrystallized, dolomitized, and argillaceous limestones, deposited in backreef and reef habitats, while Fatha formation is subdivided into several informal zones (Fig. 2), comprising anhydrite interbedded with limestone and marl. The formation is deposited in lagoonal conditions (Jassim and Goff 2006). However, the Fatha, Injana, and Bakhtiari formations represent the major seal rocks in northern Iraq (Fig. 2).

Methodology

The data for this study are kindly provided by Iraq's North Oil Company (NOC). These data sets comprise 45 stratigraphic core and cutting samples, as well as digital well logs and three crude-oil samples from six production wells (AJ-3, AJ-5, AJ-6, and AJ-13). These wells penetrated the Maudud formation's top part to depths of 2000–2500 m. In addition, 70 rock samples are acquired from AJ-8 and AJ-12 wells for palynological examination.

Thin sections are prepared for microscopic examination to determine microfacies, porosity types, and depositional environments. It included the investigation of the paleontological and petrographic components of more than 150 slides made from 45 cores and cutting samples for paleoenvironmental interpretations following the guidelines of Dunnington (1967); Embry and Klovan (1972). Grain assemblages were the primary characteristics used to distinguish Microfacies Associations (MA). Geochemical analyses are conducted at the StratoChem laboratory (Cairo, Egypt), including stable carbon isotopes and gas chromatography to describe crude-oils types and origin. Porosity and permeability determination from core samples are conducted at the north oil company laboratories (NOC), northern Iraq.

Prior to the well-log analysis, well-logging data including gamma ray, neutron, bulk density, acoustic, and resistivity logs, are digitized using neural log software, environmental corrections, and depth calibrations are done by using core information and gamma-ray log as a reference curve. Interactive Petrophysics-3.5, Surfer-16, and CorelDRAW-2021 software are used to plot calculated parameters. However, these logs are being used to evaluate the petrophysical properties of the investigated formations by substituting them into the important equations below.

M–N plot represents one of the most important parameters in the lithology determination; three logs, including density, neutron, and sonic logs, are utilized to calculate M–N values. Sonic and density data are used to determine M values, whereas neutron and density data have been used to obtain N values (Inteq 1999; Schlumberger 1972, 1989). The following parameters apply to determine the M and N values:

$$M = (DTf - DT)/(pb - pf) \times 0.01 \tag{1}$$

$$N = \left(\varnothing_N f - \varnothing_N\right)/(Pb - pf) \tag{2}$$

where $DTf = 189$ for fresh and 185 for saltwater; DT = sonic-log measurement, Pb = density log; Pf = 1.0 freshwater density; $Ø_N f = 1.0$, $Ø_N$ = neutron log porosity (NPHI).

A gamma-ray log (GR) has a direct relation with shale volume and represents an initial step in porosity calculation; a low response of gamma-ray indicates clean intervals. In order to reveal intervals with better reservoir probability, the volume of shale (V_{CL}) is estimated from a gamma-ray log (Dresser Atlas 1979), using Eq. (3 and 4).

$$I_{GR} = \frac{GRlog - GRmin}{GRmax - GRmin} \tag{3}$$

$$V_{CL} = 0.083[2^{(3.7IGR)} - 1 \tag{4}$$

where = I_{GR} = index gamma ray; GR_{log} = gamma-ray log reading, GR_{min} = minimum gamma ray, GR_{max} = maximum gamma-ray reading in shale zone.

Both of total (PHIE) and effective porosity (PHIE) of the considered formations are determined by using neutron, density, and sonic logs. Generally, the neutron log measures the direct porosity of the formation and is corrected using Eq. 5 (Zaki 1994):

$$\varnothing Ncorr. = \varnothing N - (Vsh * \varnothing Nsh) \tag{5}$$

where $Øncorr$ = neutron porosity (corrected); $ØN$ = neutron-log reading, $ØNsh$ = neutron log for shale zone. The bulk density of a rock is a function of lithology and porosity and is represented by Eq. 6 (Selley and Sonnenberg 2015):

$$\varnothing Dcorr = \frac{\left(P_{ma} - P_b\right)}{P_{ma} - P_f} - Vsh\frac{P_{ma} - P_{sh}}{p_{ma} - P_f} \tag{6}$$

where $ØDcorr$ = density porosity (corrected); ρma = matrix density (limestone = 2.71, dolomite = 2.88); ρb = log density (RHOB); ρsh = density value of shale zone; ρf = formation fluid density; ρf = 1.0 g/cc (for fresh water mud).

Sonic porosity (ØScorr) is achieved by using Eq. 7 (Dresser Atlas 1979):

$$\varnothing Scorr = \frac{\Delta t_{log} - \Delta t_{ma}}{\Delta t_f - \Delta t_{ma}} - Vsh\frac{\Delta t_{log} - \Delta t_{ma}}{\Delta t_f - \Delta t_{ma}} \tag{7}$$

where Δt Log = sonic log reading, Δtma = transit time of the matrix material (limestone = 47, dolomite = 43 µs/ft); Δtf = fresh mud = 189; and Δtsh = interval transit time for adjacent shale.

The relationship between effective porosity and total porosity is represented by the following equations:

$$PHIE = PHIT(1 - Vsh) \tag{8}$$

$$PHIT = (\varnothing Ncorr + \varnothing Dcorr)/2 \tag{9}$$

The hydrocarbon saturation can be determined using the fluid saturation property, which is expressed as the fraction or percentage of the total pore volume filled by oil, gas, or water (Tiab and Donaldson 2004, 2015). The hydrocarbon saturation is obtained by relation (10).

$$SH = 1 - SW \tag{10}$$

Water saturation (S_W) is always part of the fluids that occupy the pore spaces of reservoir rocks (Dresser

Table 1 The used parameters in permeability calculation

Wyllie-Rose method	Wyllie Rose sıvı	Swirr	b	c	kw
Timur	Oil	0.2	4.4	2	8581.0
	Gas	0.2	4.4	2	8581.0
Morris	Oil	0.2	6	2	62,500
	Gas	0.2	6	2	6241.0
Schlumberger	Oil and Gas	0.2	4.5	2	10,000.0

Atlas 1979). Water saturation (S_W) and water saturation in the flushed (S_{XO}) zones are expressed by Archie Eqs. (11 and 12):

$$S_w = \sqrt[n]{\frac{a}{\varnothing^m} \times \frac{Rw}{Rt}} \tag{11}$$

$$S_{xo} = \sqrt[n]{\frac{a}{\varnothing^m} \times \frac{Rmf}{RXO}} \tag{12}$$

where Rt = true formation resistivity (from LLD log); R_{XO} = formation resistivity in the invaded zone (from MSFL log); a = tortuosity factor (a = 1.0); n,m = 2.0; Rw = formation water resistivity, and Rmf = resistivity of the mud filtrate at formation temperature.

Water resistivity (R_W) is obtained from the spontaneous potential (sp) log using Eq. 13:

Table 2 Summary of microfacies, depositional environments, diagenesis, and pore types of reservoir rocks

Well	Formation	Depth M	Microfacies	Depo. Envi	Diagenesis	Pore Types
AJ-6	Jeribe	1024	Peneroplis Wackstone	Hypersaline lagoon	Dolomitization, recrystallization	Interparticle, intraparticle, moldic, microfractures, skeleton,
AJ-6	Jeribe	1044	Bioclastic-echinoderm packstone	Open platform	Dolomitization, dissolution	interparticle, moldic, microfractures
AJ-6	Dhiban	1073	Miliolidal mudstone	Restricted lagoon	Dolomitization, recrystallization, cementation (pore filling calcite)	Interparticle, intraparticle
AJ-6	Euphrates	1094	Peloidal packstone	Restricted lagoon	Dolomitization, recrystallization	Interparticle
AJ-6	Euphrates	1111	Foraminifera packstone	Restricted lagoon	Dolomitization, recrystallization, cementation (pore filling anhydrite)	Interparticle, intraparticle, moldic, vugs, microfractures
AJ-6	Euphrates	1130	Ooidal packstone	Winnowed (Shoal) platform	Dolomitization	intraparticle
AJ-6	Serikagni	1170	Calcareous mudstone	Outer ramp	Dolomitization, Recrystallization, dissolution, cementation (pore filling anhydrite)	Interparticle
AJ-3	Jeribe	866	Foraminiferal Mudstone-wackestone	Restricted lagoon	Dolomitization, Recrystallization, dissolution	Intercrystalline, separate vugs
AJ-3	Jeribe	870	Peneroplis bearing Wackstone			İnterparticle, intraparticle, moldic
AJ-3	Jeribe	876	Bioclastic-echinoderm bearing packstone	Restricted lagoon	Dolomitization, dissolution	
AJ-3	Dhiban	900	Miliolidal mudstone	Restricted lagoon	Dolomitization, recrystallization, cementation (anhydrite)	İnterparticle, moldic, microfractures
AJ-3	Euphrates	925	Peloidal packstone	Restricted lagoon		İnterparticle, intraparticle, moldic,
AJ-3	Euphrates	934	Foraminifera packstone		Dolomitization, recrystallization	
AJ-3	Euphrates	975	Ooidal packstone	Winnowed platform	Dolomitization, dissolution	microfractures
AJ-3	Serikagni	1010	Calcareous mudstone	Outer ramp	Dolomitization, cementation (anhydrite)	
AJ-13	Jeribe	1173	Foraminiferal mudstone-wackestone	Restricted lagoon	Dolomitization, dissolution	İnterparticle, intraparticle, moldic, microfractures
AJ-13	Jeribe	1190	Peneroplis bearing wackestone			
AJ-13	Dhiban	1220	Calcareous mudstone		Dolomitization, cementation (calcite)	microfractures
AJ-13	Euphrates	1245	Foraminifera packstone			
AJ-13	Euphrates	1299	Ooidal packstone	Winnowed (Shoal) platform		İnterparticle, intraparticle
AJ-13	Serikagni	1315	Calcareous mudstone	Outer ramp	Dolomitization, recrystallization cementation	Dolomitization, Microfractures

$$\mathrm{Sp} = -(60 + 0.133\mathrm{T})\log\frac{\mathrm{Rmf}}{\mathrm{Rw}} \quad (13)$$

where = –(60 + 0.133 T) = is the constant; T = is the formation temperature in F°.

The bulk volume water is the product of porosity and water saturation (Tiab and Donaldson 2004, 2015):

$$B_{VW} = \varnothing e S_W \quad (14)$$

$B_{VW}S_{XO} = S_{XO}\varnothing$ (15) Permeability estimated using Wylie and Rose equation (Wyllie and Rose 1950):

$$K = kw\frac{Phi^b}{Swi^c} \quad (16)$$

The Wylie and Rose component is summarized in Table 1. The neural network (ANN) is applied for uncored zones to obtain porosity and permeability from log data, the standard method to calculate permeability is described by Haykin (2009), and it is represented as follows:

$$y_{net} = \sum_{i=1}^{n} x_i w_i + w_b \quad (17)$$

$$y_{out} = \int (net) = \left(1 + e^{-ynet}\right)^{-1} \quad (18)$$

where ynet = summation of weighted input; xi = is the neuron input, wi = is a weight associated with each neuron input; wb = bias, and n = number of samples; yout = is the response of the neural network system.

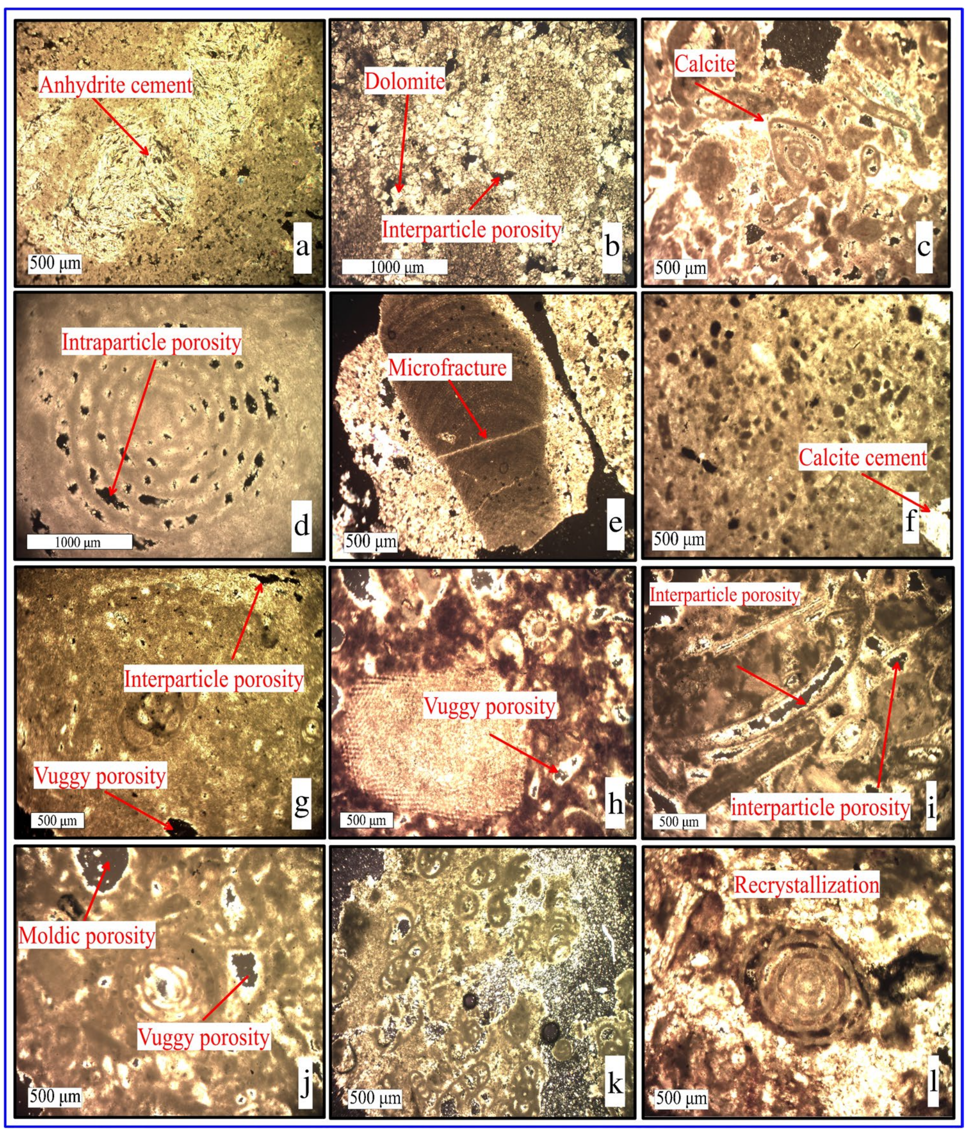

Fig. 3 Microfacies and porosity types of Tertiary succession

Results and discussion

Microfacies and depositional environment

Eight different microfacies types are recognized in the Serikagni, Euphrates, Dhiban, and Jeribe formations based on the microscopic examination (Table 2).

The typical classification of microfacies is described by Dunham (1962). There was one microfacies type in the Serikagni and Dhiban formations, three distinct microfacies types in the Euphrates formation, and two distinct microfacies types in the Jeribe formation (Fig. 3), the main depositional environments of studied formations ranged from the lagoon (hypersaline) to the open platform.

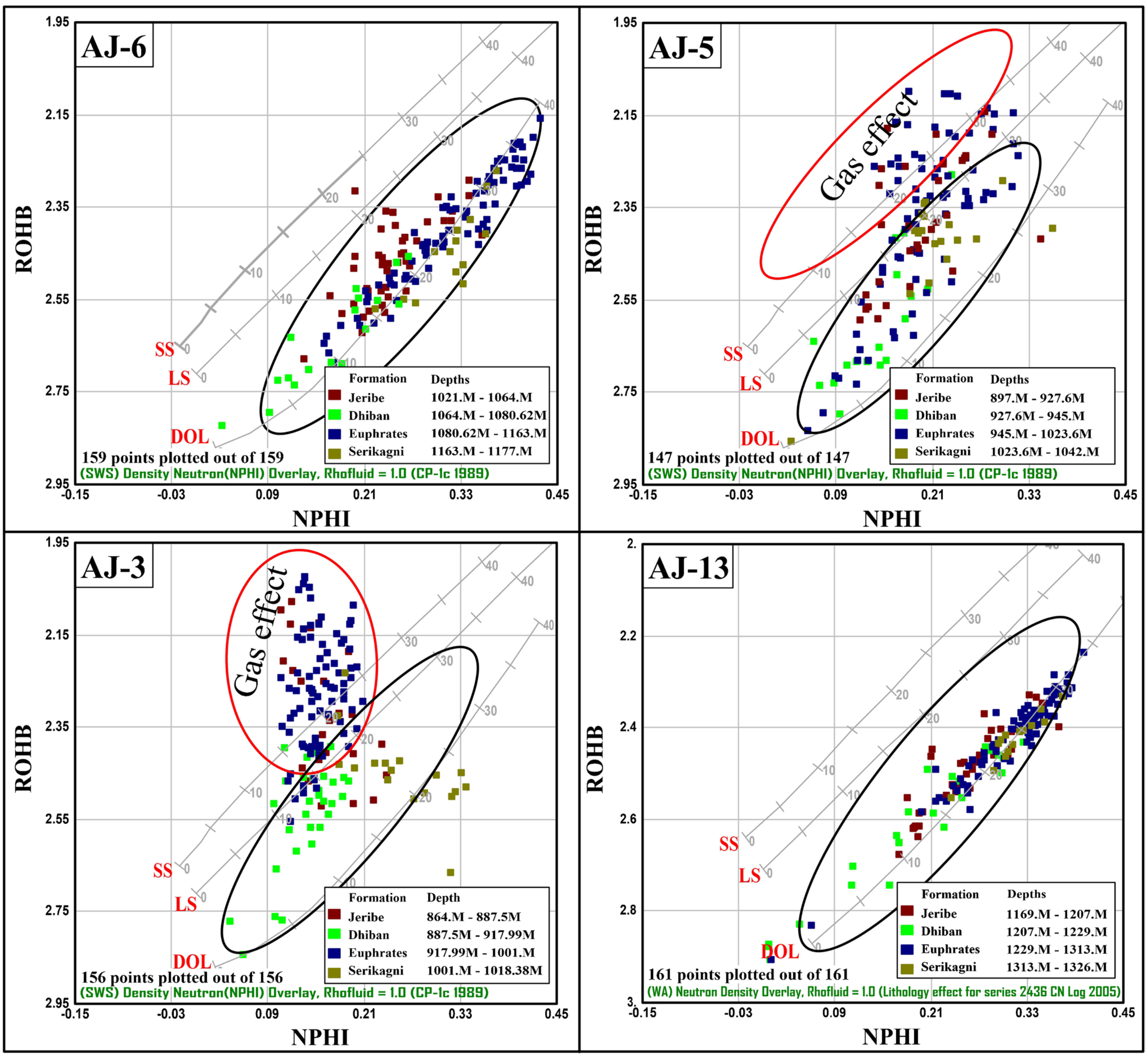

Fig. 4 Neutron–density cross-plot of AJ-6, AJ-5, AJ-3, and AJ-13 wells

Dolomitization, recrystallization, cementation, and dissolution are the four major kinds of diagenesis in the investigated formations (Tucker and Wright 1990; Flügel 2004). Several porosity types were distinguished based on Choquette and Pray (1970) method including interparticle, intraparticle, moldic, microfractures, and vuggy porosity types (Fig. 3; Table 2).

Lithological assessment

Well-logs reflect direct and indirect measures of rock properties, providing the possibility to determine groups of rocks with particular characteristics that distinguish them from other rock types. Relations between electrical log responses were studied to define how many rock types

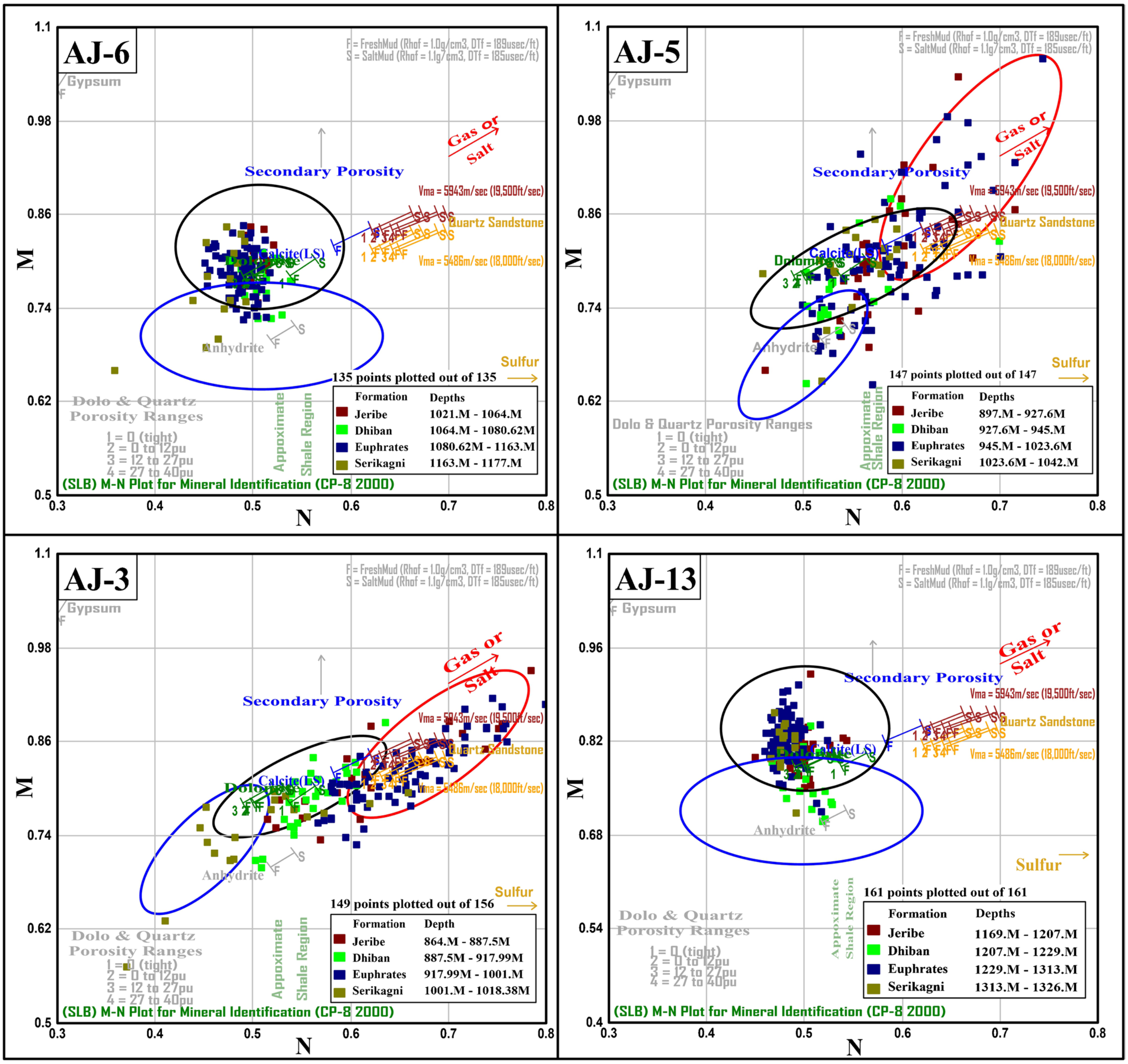

Fig. 5 M–N cross-plot of AJ-6, AJ-5, AJ-3, and AJ-13 wells

Table 3 Petrophysical parameters averages of Tertiary reservoir rocks, NE Iraq

Formation	Well	VCLGR (%)	PHIT (%)	PHIE (%)	PhiSon (%)	S_W (%)	S_{XO} (%)	B_{VW} (%)	$B_{VW}S_{XO}$ (%)
Jeribe	AJ-6	27	12.5	6.6	17.4	41	47.8	0	2.9
Jeribe	AJ-5	17	15.7	13.9	22	22	55.9	0	6.3
Jeribe	AJ-3	14.5	21.5	21.5	22.5	21.3	43.5	6.9	6.3
Jeribe	AJ-13	16.8	31	26.2	15.5	100	100	39.7	26.1
Dhiban	AJ-6	7.5	10.2	7.2	11.6	63	72.5	3.3	4.6
Dhiban	AJ-5	5.1	4.6	3.6	14.3	77.3	89.8	1.1	2.3
Dhiban	AJ-3	0.7	10.1	10.1	14.7	49	65	2.6	4.5
Dhiban	AJ-13	1	31	28.2	13	96.2	96.2	26.5	26.5
Euphrates	AJ-6	8.7	21.6	18.6	22.4	75	77.4	14.2	14.7
Euphrates	AJ-5	6	16.2	15.5	22.6	29	64.8	2.1	8.6
Euphrates	AJ-3	5.5	23	23	25.1	11.5	35.4	2	6.8
Euphrates	AJ-13	6.8	37.7	30	17.6	99	100	34.6	34.6
Serikagni	AJ-6	20.4	17.5	12.2	20.3	94	98.2	11.4	12
Serikagni	AJ-5	19.9	14.4	12.2	20.5	41	61.5	4.9	7.7
Serikagni	AJ-3	21.3	11.6	11.6	22.7	69.2	79.2	6.9	8.3
Serikagni	AJ-13	3	30	27	18.2	100	100	39.7	39.7

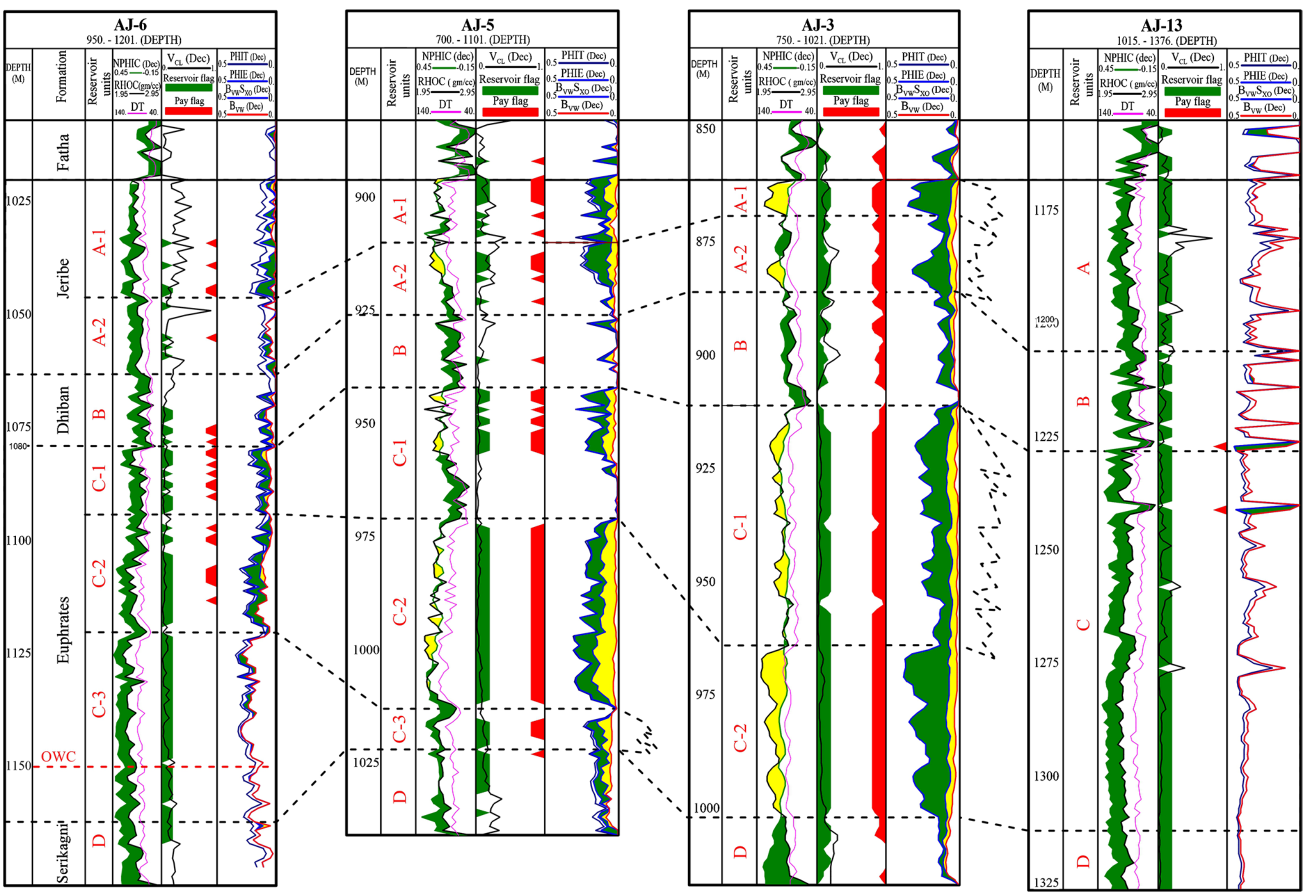

Fig. 6 Petrophysical results and main reservoir units in the studied wells

can be determined and what specific characteristics they have that are particular to them. This analysis allows the definition of four petrophysical rock types (Figs. 4 and 5). The neutron–density (N-D) and M–N cross-plots can be used to identify lithologies such as dolomite, limestone, quartz, and evaporites (Schlumberger 1989). Moreover, to distinguish oil and gas (Asquith and Krygowski 2004; Kennedy 2015). The N-D cross-plots (CP-le Chart) suggest that the main lithologies of Serikagni, Euphrates, Dhiban, and Jeribe formations are limestone and dolomitic limestone, which becomes more dolomitized in AJ-6 and AJ-13 wells. The results were compared to surface and underground stratigraphic studies (e.g., Dunnington 1967; Buday 1980a; Jassim and Goff 2006; Al-Dabbas et al. 2013; Sissakian et al. 2016; Ahmed et al. 2021), and the correlation results showed a similarity relation of more than 85%. The neutron–density cross-plots revealed that the Euphrates and Jeribe formations contain larger amounts of hydrocarbon than Serikagni and Dhiban formations (Fig. 4). Based on the M–N cross-plots (Fig. 5), the Serikagni and Euphrates formations consist of dolomite and calcite, while Dhiban formation comprises calcite, anhydrite, and dolomites, whereas calcite and dolomite represent the main constituents of the Jeribe formation with a little anhydrite. The scattered data points of Euphrates and Jeribe formations in AJ-5 and AJ-3 are due to the hydrocarbon contents (Fig. 5). This first model improves the prediction of lithologies in the studied area, especially in uncored wells, using well-log measurements.

Clay and Porosity contents

The higher reserve quality the lower the clay contents, generally shale volume represents one of the most important factors that affect porosity values. However, the lowermost shale content in the Euphrates and Dhiban formations, shale volume (V_{CL}) ranged between 0.7 and 7.5% and 5.5 and 8.7%, respectively, while in Serikagni and

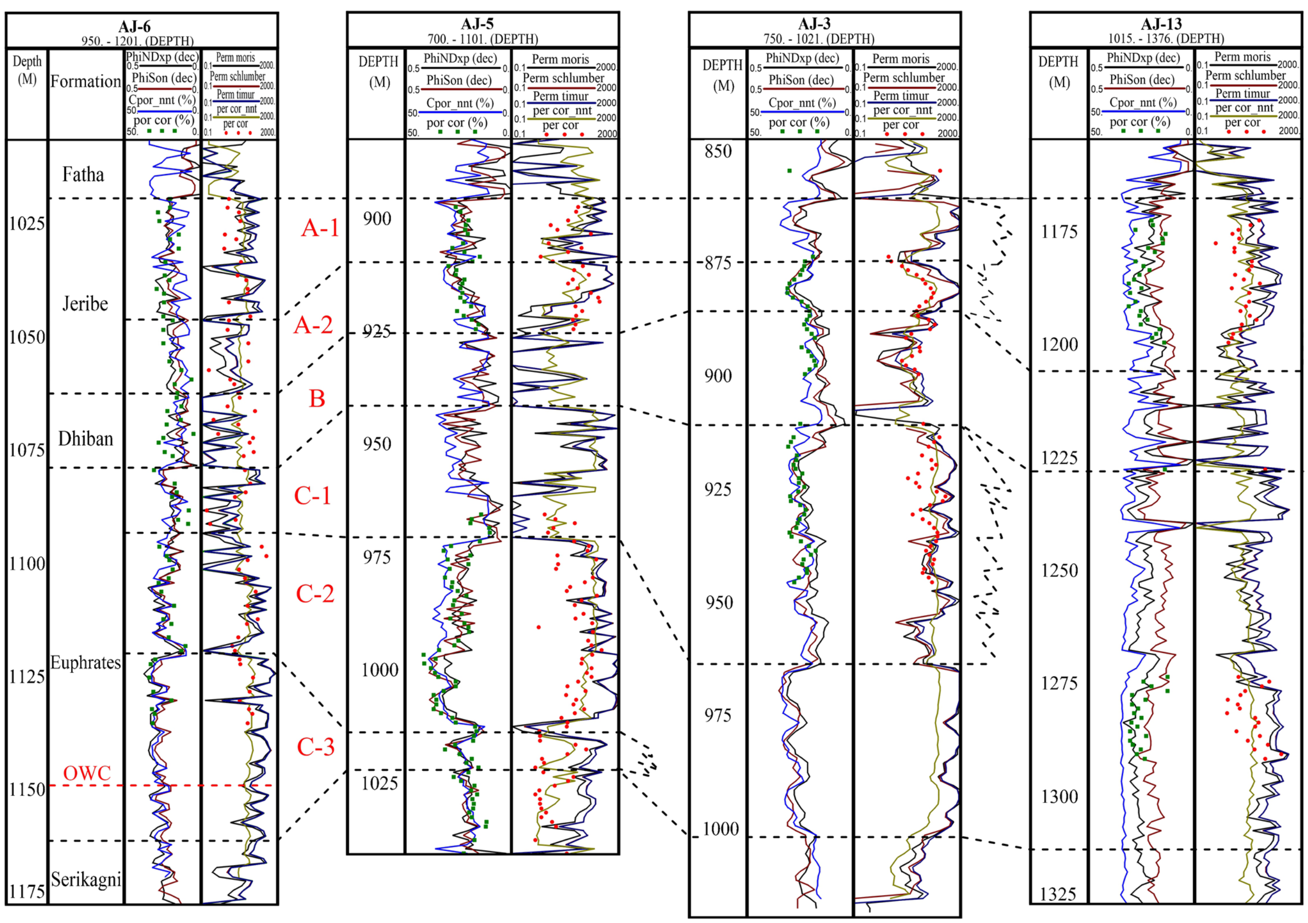

Fig. 7 Correlation between porosity and permeability through studied wells

Jeribe formations, ranged between 14.5 and 27% and 3.0 and 20.4%, respectively (Table 3), these values showed a good reserve quality of mentioned formations except lower parts of Serikagni formation (Fig. 6). Porosity is the proportion of voids in the rocks and represented as a percentage or a decimal fraction, the matrix porosity rather than vuggy or fracture porosity calculated by sonic log (Asquith and Krygowski 2004). Sonic porosity values reached 25.1% for Serikagni, Euphrates, and Jeribe formations as an effect of dolomitization and dissolution; these values reduce in Dhiban formation, which ranged between 11.6 and 14.7% indicating cementation and anhydrite contents (Fig. 6). The average values of the PHIT and PHIE porosities ranged between 10.1 and 32.7% and 3.6 and 30.0% (Table 3), respectively.

Hydrocarbon estimation

The water saturation (S_W) is the proportion of brine rather than hydrocarbon captured in pore space, which affects hydrocarbon quantity and movements (Ellis and Singer 2007). The water resistivity (Rw) values ranged between 0.04 and 0.05 in all wells except in AJ-13 which is below oil–water contact. Average values of the bulk volume of water (B_{VW}) ranged between 0 and 39.7%, while in the flushed zones ($B_{VW}S_{xo}$), ranged between 23 and 39.7% (Fig. 6), the combination of S_{xo}, Sw, bulk volume of water gives some qualitative indication of permeability and the movable hydrocarbons saturation, where the water saturation in the flushed zone (S_{xo}) indicates movable hydrocarbons (Dresser Atlas 1979; Hakimi et al. 2012; Mamaseni et al. 2018). The lower water saturation (S_W) values in an invaded zone than water saturation (S_{XO}) in the flushed zone (Table 3), indicates that the Euphrates and Jeribe formations have a good reservoir quality and high hydrocarbon contents, while Serikagni, Dhiban formations have higher water and lower hydrocarbon contents (Fig. 6).

Permeability and net pay

The Wylie-Rose and neural network (ANN) methods are used to estimate permeability values. The neural network is a computational model that simulates the function of the human nervous system (Haykin 2009). This method is mentioned by many authors (Handhel 2009; Bhatt and Helle 2010; Verma et al. 2014; Kohli and Arora 2016). The permeability estimation from log data in the uncored zones is an important parameter for evaluation purposes and hydrocarbon-bearing zones identification. The main results of porosity and permeability are summarized in Fig. 7, the porosity and permeability values have revealed good to excellent reserve capability of Euphrates and Jeribe formations, while Serikagni, Dhiban, and the lower part of Fatha (Transition)

Table 4 Geochemical parameters results of crude-oil samples from reservoir rocks, NE Iraq

Well	Source Rocks	Depth M	SAT. wt.%	ARO. wt.%	NSO. wt.%	ASP. wt.%	$\delta^{13}C$ SAT	$\delta^{13}C$ ARO	Pri/Phy	Pri/n-C_{17}	Phy/n-C_{18}	S	API
AJ-31	Jeribe	800–900	61.6	29.7	2.58	6.19	-27.3	-27.4	0.91	0.29	0.38	2.85	33
AJ-17	Euphrates	850–1000	56.02	21.6	20.72	1.65	-27.4	-27.4	0.8	0.25	0.37	2.87	31
AJ-12	Serikagni	2250 – 2350	61.77	20.4	14.73	3.08	-27	-27.3	0.8	0.16	0.22	2.61	32

$\delta^{13}C_{SAT.}$=Composition of stable carbon for the saturated hydrocarbon portion; $\delta^{13}C_{ARO.}$=composition of stable carbon of the aromatic hydrocarbon portion; Pri./Phy.=ratio of pristane/phytane; Pri/n-C_{17}=ratio of pristane/n-C_{17}; Phy/n-C_{18}=ratio of phytane/n-C_{18}; canonical variable (CV.)=−2.53$^{13}\delta C_{SAT.}$+2.22 $\delta^{13}C_{ARO.}$−11.65; S.=sulfur content of crude-oil; American Petroleum Institute (API) to measure crude-oil gravity=(141.5/specific gravity)−131.5

formations have poor to fair hydrocarbon reserve quality. The net pay and net/gross values obtained from porosity, permeability, and water saturation data, represent the most important petrophysical parameters that remark hydrocarbon-bearing zones. The reservoir rocks were divided into eight reservoir units, based on different petrophysical parameters such as porosity, permeability, water/hydrocarbon saturation, and a bulk volume of water was applied to establish reservoir and non-reservoir units (Fig. 6).

Crude-oil evaluation

The geochemical data of 3 crude-oil samples from the Tertiary reservoirs are shown in Table 4; Fig. 8; these data were used to determine depositional conditions of organic matter and crude-oils origins (Peters and Moldowan 1993). The saturates, aromatics, resins, and asphaltenes values were used to determine the depositional environment of organic matter and crude-oil origin (Tissot and Welte 1984; Al-Khafaji et al. 2020, 2021; Kong et al. 2020), and the analyzed crude-oil samples (Table 4; Fig. 8C) are paraffinic (marine origin) type. Furthermore, the saturate and aromatic fractions of $\delta^{13}C$ used to determine marine and terrestrial origin organic matters (Sofer 1984), which ranged between -27.4 and -27% and -27.4 and -27.3% (Table 4; Fig. 8C), revealing that the crude-oil samples are generated mainly from marine origin source rocks. The relationship between Pr/n-C_{17} and Ph/n-C_{18} (Table 4; Fig. 8D) revealed a reducing environment with kerogen type-II. Higher API values of up to 33 indicate medium-light crude-oil type. Based on Hsu and Robinson's (2019) classification, higher sulfur contents are reached 1.5%, indicating sour crude-oil type in Mesopotamian Basin, northern Iraq. The pristane/phytane ratio provides information about the environment, regard to lithology, and the maturity of hydrocarbons (Peters and Moldowan 1993). Low pristane/phytane values < 1.0 indicate marine

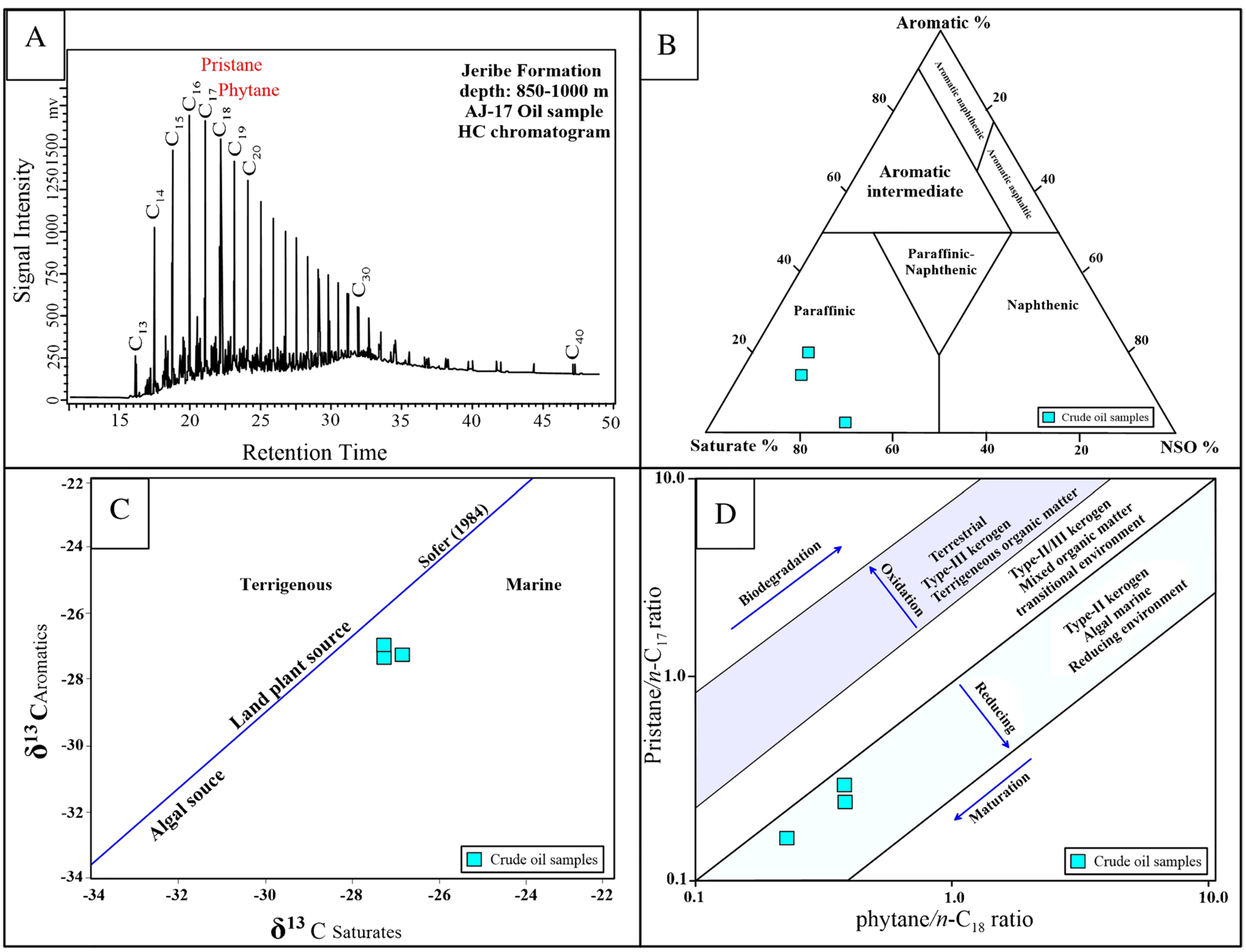

Fig. 8 **A** Representative gas chromatography (GC) of crude-oils from reservoir rocks, **B** Ternary diagram of aromatic, saturate, and NSO components presenting crude-oils type in the Mesopotamian Basin. **C** Saturate and the aromatic fraction of carbon isotope cross-plot (Sofer 1984). **D** Pristane/n-C_{17} versus phytane/n-C_{18} for crude-oils from the Tertiary reservoir (Peters and Moldowan 1993)

depositional environments, while higher values reveal terrestrial depositional conditions (Powell and McKirdy 1973; ten Haven et al. 1987; Abeed et al. 2012; Al-Khafaji et al. 2021). However, the analyzed samples have low Pri./Phy. up to 0.99 (Table 4) and indicate reducing conditions and contributions of marine origin organic matter.

Palynofacies assessment

Palynological investigation of 70 core and cutting samples from Jurassic–Cretaceous source rocks has indicated that the Sargelu, Naokelekan, Gotnia, and Chia Gara formations are dominated by amorphous-organic matters (AOM) of up to 80%, with rare palynomorphs and phytoclasts contents of up to 20%. Tyson's (1993) APP ternary diagram and Thompson and Dembicki's (1986) AOM categorization are used to identify kerogen and depositional environments. In this study, the palynomorphs contain dinoflagellate cysts, foraminiferal test linings, and fungi (Fig. 9). Meanwhile, phytoclasts consist of terrestrial origin tracheids and cuticles, with few marine inhibitors such as Scolecodonts (Fig. 9).

The Sargelu formation's palynofacies are characterized by thin-bedded, black, bituminous limestone, dolomitic limestone, and black papery shale layers. The studied samples include a modest amount of phytoclasts (up to 9%) and a significant amount of marine-derived AOM (up to 90% of total organic matter), as well as palynomorphs (up to 24%).

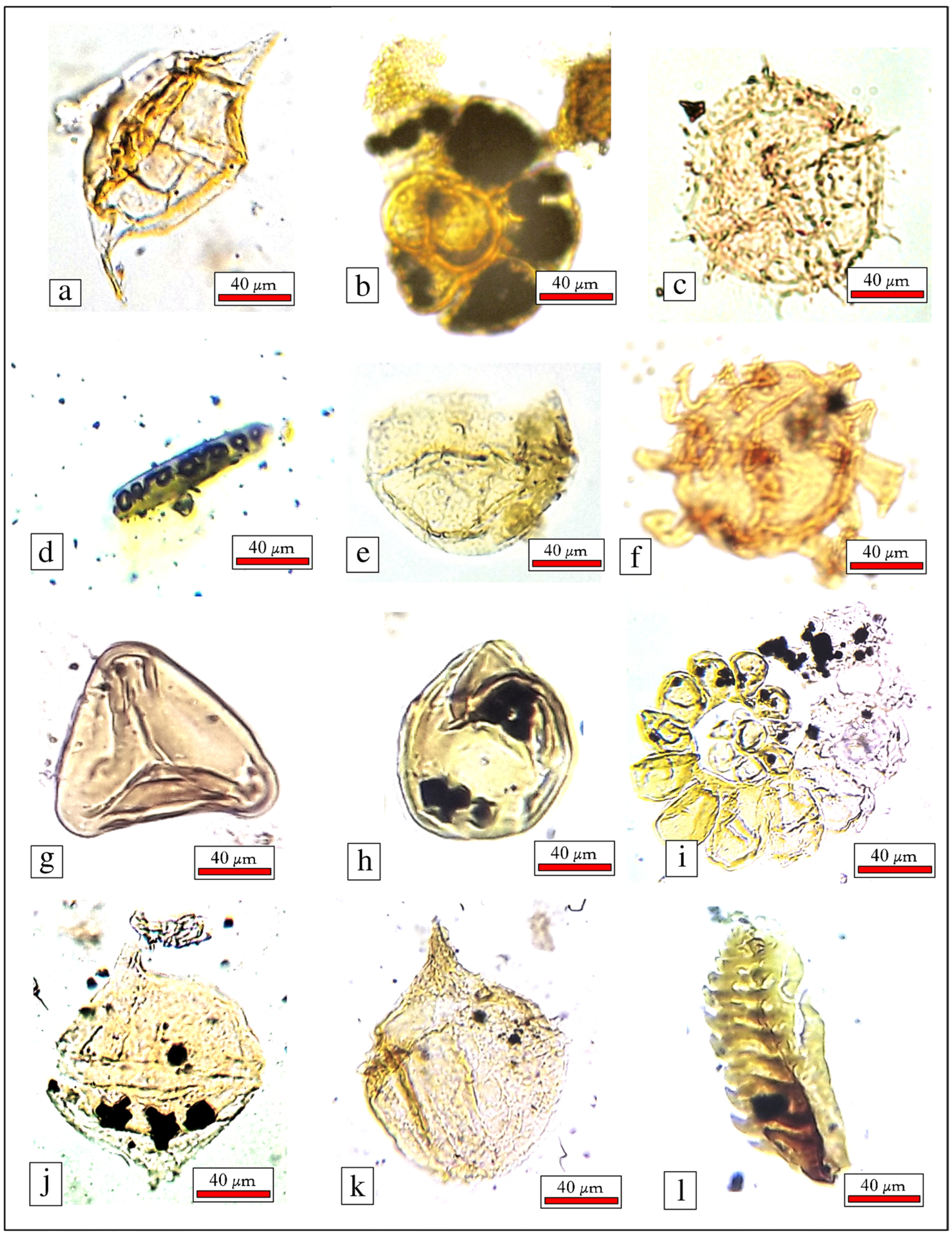

Fig. 9 Palynomorphs from the Sargelu, Naokelekan, Chia Gara formations in Ajeel oilfield, NE Iraq. **a** *Muderongia* sp. dinocyst specimen, AJ-12 well, Sargelu formation, 3575 m., **b** Foraminiferal test linings, AJ-12 well, Sargelu formation, 3550 m., **c** *Sentusidinium* sp., dinocyst specimen, AJ-12 well, Sargelu formation, 3510 m., **d** Fungal spore sac, AJ-12, Sargelu formation, 3300 m., **e** *Meiourogonyaulax cytogenesis*, Upper Callovian, AJ-8 well, Naokelekan formation, 3240 m., **f** *Compositosphaeridium* sp, dinocyst, AJ-8 well, Naokelekan formation, 3238 m., **g** *Gleichenidites* sp. dinocyst specimen, Middle Jurassic, AJ-12 well, Naokelekan formation, 3496 m., **h** *Chytroeisphaeridia chytroeides*, dinocyst specimen, Lower Callovian, AJ-8 well, Naokelekan formation, 3238 m., **i** Foraminiferal test linings, AJ-12 well, Chia Gara formation, 3317 m., **j** *Cribroperidinium longicornis*. dinocyst specimen, AJ-12 well, Chia Gara formation, 3310 m., **k** *Cribroperidinium edwardsii*, dinocyst specimen, AJ-8 well, Chia Gara formation, 3125 m., **l** *Unidentified Scolecodonts,* AJ-8 well, Chia Gara formation, 3280 m

The palynomorphs including *Muderongia* sp., foraminiferal test linings, *Sentusidinium* sp., and fungal spore sacs indicate Bajocian-Bathonian age and outer neritic deeper marine environment.

The Naokelekan formation's palynofacies are observed in laminated shaly limestone, hard dark gray limestone, and thin-bedded, bituminous limestone with intercalated black bituminous-calcareous shale. All examined samples are dominated by AOM at a content of up to 95%, with rare phytoclasts at a concentration of up to 7%. Overall ratio of palynomorphs was between 5 and 9%, consisting of *Meiourogonyaulax cytogenesis*, *Compositosphaeridium* sp., and *Gleichenidites* sp., suggesting that this formation was Callovian-Kimmeridgian in age (Fig. 9).

The Gotnia is composed of anhydrite that is interbedded by brown calcareous shales, thin black bituminous shales, and recrystallized limestone beds. All of the examined samples contain a significant amount of AOM, up to 98%. Furthermore, palynofacies of the Chia Gara formation are determined in limestone, calcareous shale, argillaceous limestone, and shale beds. All of the examined samples have domination by AOM usually more than 90%, indicating suboxic to anoxic sedimentation conditions (Tyson 1995). The palynomorphs represented by foraminiferal test linings, *Cribroperidinium longicornis*, *Cribroperidinium edwardsii*, and Scolecodont (Fig. 9), indicate Tithonian-Berriasian age and mid-deep shelf depositional environment.

Plotting the organic-matter assemblage ratios on Tyson's (1993, Fig. 10) APP ternary diagram indicates a transition from a distal suboxic-anoxic to a distal dysoxic–oxic environment, owing to the high content of AOM, which dilutes

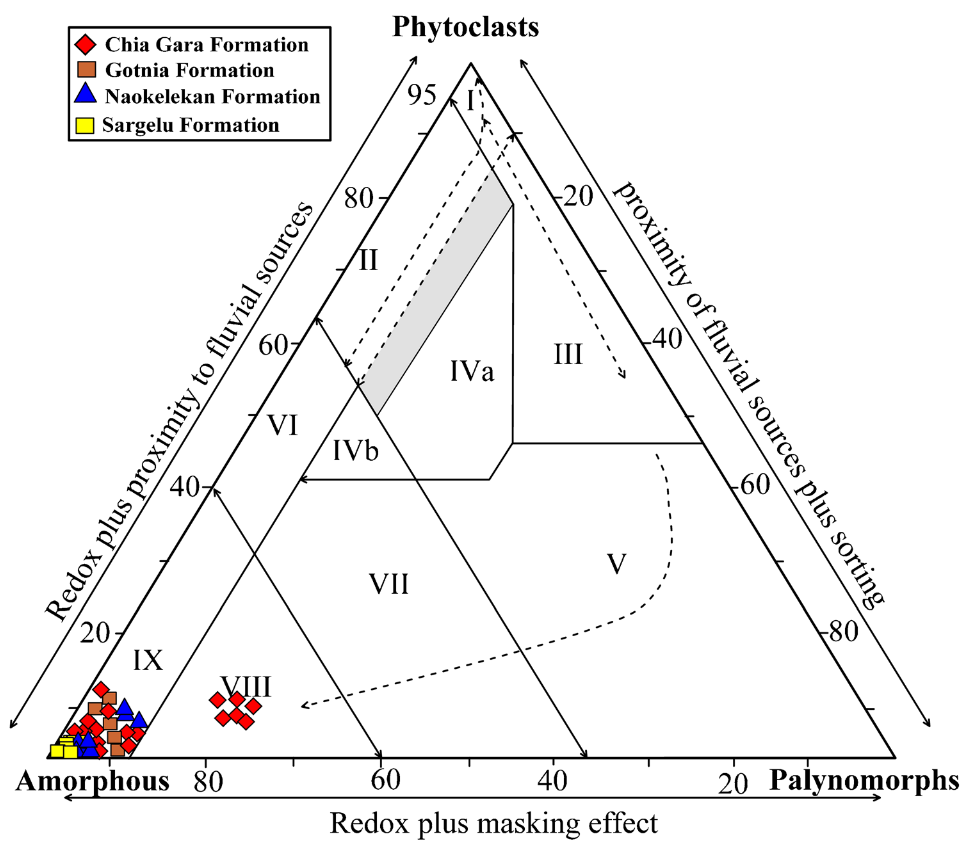

Palynofacies fields	Environment of deposition	Kerogen type
I	Highly proximal shelf or basin.	Type-III (Gas-prone)
II	Marginal dyoxic- anoxic basin	Type-III (Gas-prone)
III	Heterolithic oxic shelf (proximal shelf).	Type-III or -IV (Gas-prone)
IV	Shelf to basin transition.	Type-III or -II (Gas-prone)
V	Mud dominated oxic shelf (distal shelf).	Type-III > -IV (Gas-prone)
VI	Proximal suboxic- anoxic shelf.	Type-II (Oil-prone)
VII	Distal dysoxic- anoxic shelf.	Type-II (Oil-prone)
VIII	Distal dysoxic- oxic shelf.	Type-II > -I (Oil-prone)
IX	Distal suboxic- anoxic basin.	Type-II >-I (Highly oil-prone)

Fig. 10 Ternary diagram of palynofacies groups is used for paleoenvironmental analyses and kerogen types determination (Tyson 1995)

all other organic particles and is consequently classified as Type II > I kerogen (highly oil prone).

Conclusions

The microscopic examination (Table 4) has revealed that the Serikagni formation is deposited in the outer-ramp environment, while other formations are deposited in the inner ramp environment.

The N-D and M–N cross-plots show that Tertiary formations consist of limestone, dolomite, dolomitic limestone, marly limestone, and anhydrite. The Euphrates and Jeribe formations are separated by Dhiban evaporite units. Moreover, the anhydrite ($CaSO_4$) has a low gamma response, neutron porosity of up to 2%, and a bulk density of 2.98 gm/cc (Fig. 6). The porosity and permeability results show good reserve qualities in the C2, A2 units, and partially in the C3, C1, A1 units, and the hydrocarbons have been reserved between 860 and 1150 m, while fair reservoir quality in the D and B units due to anhydrite and shale content (Fig. 6). The geochemical results of crude-oils from Mesopotamian Basin, northern Iraq, recognized medium-light type, which is originated mainly from marine origin organic matters.

Palynofacies examination revealed that the Sargelu, Naokelekan, and Gotnia formations have been deposited primarily in the distal suboxic–anoxic conditions and contain kerogen type II (oil window), while Chia Gara formation deposited mainly in the distal suboxic–anoxic and distal dysoxic–oxic conditions and contain Type-II>I (oil-prone), suggesting that the Jurassic–Cretaceous successions are main oil sources in the Mesopotamian Basin, northern Iraq.

Acknowledgements The authors acknowledge and appreciate very much the North Oil Company (Kirkuk, Iraq) for providing technical support, research material, and documentation.

Declarations

Conflict of interest The authors have no conflicts of interest to declare that are relevant to the content of this article.

References

Abdullah HG, Collier REL, Mountney NP (2019) The palaeoshoreline of Early Miocene formations (Euphrates and Jeribe) at the periphery of the Zagros Foreland Basin, Sulaimani Governorate, Kurdistan Region, NE Iraq. Arab J Geosci 12:574. https://doi.org/10.1007/s12517-019-4716-2

Abeed AT, Lazim SA, Hamied RS (2019) Modeling of Petrophysical Properties and Reserve Estimation of Mishrif Formation-Garraf Oil Field. IOP Conf Ser Mater Sci Eng 579:012037. https://doi.org/10.1088/1757-899x/579/1/012037

Abeed Q, Leythaeuser D, Littke R (2012) Geochemistry, origin and correlation of crude oils in Lower Cretaceous sedimentary sequences of the southern Mesopotamian Basin, southern Iraq. Org Geochem 46:113–126. https://doi.org/10.1016/j.orggeochem.2012.02.007

Ahlbrandt TS, Pollastro RM, Klett TR et al (2000) Region 2 Assessment Summary — Middle East and North Africa. U S Geol Surv Digit Data Ser 60:46

Ahmed KM, Hassan FN, Faisal SH (2021) Petrography and Microfacies of Ghar and Euphrates Formations in the Busaiya area in Southern Iraq. Rev Int Geogr Educ Online 11:4809–4825

Al-Ameri T, Zumberge J (2013) Middle and Upper Jurassic hydrocarbon potential of the Zagros Fold Belt, North Iraq. Mar Pet Geol 36:1–22

Al-Dabbas MA, Al-Sagr KEA, Al-Jassim JA, Al-Jwaini YS (2013) Sedimentological and diagenetic study of the Early Middle Miocene Jeribe Limestone Formation in selected wells from Iraq northern oilfields (Ajil; Hamrin; Jadid; Khashab). Baghdad Sci J 10:207–216. https://doi.org/10.21123/bsj.10.1.207-216

Al-Dabbas MA, Hassan RA (2013) Geochemical and palynological analyses of the Serikagni Formation, Sinjar, Iraq. Arab J Geosci 6:1395–1406. https://doi.org/10.1007/s12517-011-0451-z

Al-Fandi EI, Malak ZA, Hadid NA (2020) Sequence stratigraphy, depositional environments and reservoir characterization of sa'di formation in east Baghdad and halfiya oilfields. Iraqi Geol J 53:21–35. https://doi.org/10.46717/igj.53.1c.2rx-2020-04-02

Al-Khafaji AJ, Hakimi MH, Ibrahim E-K et al (2020) Organic geochemistry of oil seeps from the Abu-Jir Fault Zone in the Al-Anbar Governorate, western Iraq: Implications for early-mature sulfur-rich source rock. J Pet Sci Eng 184:106584. https://doi.org/10.1016/j.petrol.2019.106584

Al-Khafaji AJ, Hakimi MH, Mohialdeen IMJ et al (2021) Geochemical characteristics of crude oils and basin modelling of the probable source rocks in the Southern Mesopotamian Basin, South Iraq. J Pet Sci Eng 196:107641. https://doi.org/10.1016/j.petrol.2020.107641

Al-Khafaji AJ, Hakimi MH, Najaf AA (2018) Organic geochemistry characterisation of crude oils from Mishrif reservoir rocks in the southern Mesopotamian Basin, South Iraq: Implication for source input and paleoenvironmental conditions. Egypt J Pet 27:117–130. https://doi.org/10.1016/j.ejpe.2017.02.001

Al-Khafaji AJ, Al NFM, Al IRN, Sadooni FN (2019) Geochemical investigation of Yamama crude oils and their inferred source rocks in the Mesopotamian Basin, Southern Iraq. Pet Sci Technol 37:2025–2033. https://doi.org/10.1080/10916466.2019.1578801

Alsharhan AS, Nairn AEM (1997) Sedimentary basins and petroleum geology of the Middle East. Elsevier

Altameemi AMH, Alzaidy A (2018) Formation Evaluation by using Well Logging of Mishrif Formation in the Noor Oil Field, Southeast Iraq. Iraqi J Sci 59:144–155. https://doi.org/10.24996/ijs.2018.59.1a.16

Ameen MS (1992) Effect of Basement Tectonics on Hydrocarbon Generation, Migration, and Accumulation in Northern Iraq. Am Assoc Pet Geol Bull 76:356–370. https://doi.org/10.1306/BDFF87FE-1718-11D7-8645000102C1865D

Asquith G, Krygowski D (2004) Basic well log analysis, second. American Association of Petroleum Geologists

Badics B, Aqrawi A (2015) Geochemical characterisation, volumetric assessment and shale-oil/gas potential of the Middle Jurassic-Lower Cretaceous source rocks of NE Arabian Plate. Geoarabia-Manama 20:99–140

Bellen RC van, Dunnington H V, Wetzel R (1959) Lexique stratigraphique international: Asie. 10.a. Iraq, III

Beydoun ZR (1991) Arabian plate hydrocarbon geology and potential. A plate tectonic approach, 6th edn. The American Association of

Petroleum Geologists, Tulsa, Oklahoma. https://doi.org/10.1306/St33533
Bhatt A, Helle HB (2010) Determination of facies from well logs using modular neural networks. Pet Geosci 8:217–228. https://doi.org/10.1144/petgeo.8.3.217
Buday T (1980a) The regional geology of Iraq, vol 1: stratigraphy and paleogeography. Publications of Geological Survey of Iraq, Baghdad, p 445
Buday T (1980b) The regional geology of Iraq. Geological Survey of Iraq, Baghdad. https://doi.org/10.1017/CBO9781107415324.004
Choquette PW, Pray LC (1970) Geologic Nomenclature and Classification of Porosity in Sedimentary Carbonates. Am Assoc Pet Geol Bull 54:207–250. https://doi.org/10.1306/5D25C98B-16C1-11D7-8645000102C1865D
Ctyrokey P, Karim AK (1971) Stratigraphy and paleontology of the Oligocene and Miocene strata near Anah, Euphrates valley, west Iraq. GEOSURV
Dresser Atlas (1979) Log interpretation charts. Dresser Atlas, Dresser Industries
Dunham RJ (1962) Classification of Carbonate Rocks According to Depositional Texture. Classif Carbonate Rocks—A Symp 1:12
Dunnington HV (1967) Stratigraphical distribution of oilfields in Iraq-Iran-Arabia Basin
Ellis DV, Singer JM (2007) Well logging for earth scientists. Springer Netherlands
Embry AF, Klovan JE (1972) Absolute water depth limits of Late Devonian paleoecological zones. Geol Rundschau 61:672–686
Flügel E (2004) Microfacies of Carbonate Rocks, Analysis Interpretation and Application. Springer Berlin Heidelberg, Berlin
Gharib AF, Özkan AM, Hakimi MH et al (2021) Integrated geochemical characterization and geological modeling of organic matter-rich limestones and oils from Ajeel Oilfield in Mesopotamian Basin, Northern Iraq. Mar Pet Geol 126:104930. https://doi.org/10.1016/j.marpetgeo.2021.104930
Hakimi MH, Shalaby MR, Abdullah WH (2012) Application of well log analysis to assess the petrophysical parameters of the Lower Cretaceous biyad formation, East Shabowah Oilfields, Masila Basin, Yemen. World Appl Sci J 16:1227–1238
Hamdullaa SM, Hassanb AH, Tawfiq YJ (2018) Building geological model for tertiary reservoir of exploration Ismail oil field, North Iraq. Iraqi J Chem Pet Eng 19:1–7
Handhel AM (2009) Prediction of Reservoir Permeability From Wire Logs Data Using Artificial Neural Networks. Iraqi J Sci 50:67–74
Haykin S (2009) Neural networks and learning Machines, 3rd edn. Pearson Education, New York
Horn M (2003) Selected features of giant fields, using maps and histograms. AAPG Bull (United States) 1868(78):340
Horn M (2004) Selected features of giant fields, using maps and histograms. 10068
Hsu CS, Robinson PR (2019) Petroleum science and technology, 1st edn. Springer International Publishing. https://doi.org/10.1007/978-3-030-16275-7
Hussein D, Collier R, Lawrence JA et al (2017) Stratigraphic correlation and paleoenvironmental analysis of the hydrocarbon-bearing early Miocene Euphrates and Jeribe formations in the Zagros folded-thrust belt. Arab J Geosci 10:543. https://doi.org/10.1007/s12517-017-3342-0
Inteq BH (1999) Petroleum geology. Thorne Houston, New York
Jassim SZ, Buday T (2006) Tectonic framework. In: Jassim SZ, Goff JC (eds) Geology of Iraq. Dolin, Prague and Moravian Museum (Brno), Czech Republic, pp 45–55
Jassim SZ, Goff JC (2006) Geology of Iraq, 1st edn. DOLIN, s.r.o., distributed by Geological Society of London. https://doi.org/10.1007/s13398-014-0173-7.2
Kennedy M (2015) Practical petrophysics. Elsevier. https://doi.org/10.1016/B978-0-444-63270-8.00001-3
Kohli A, Arora P (2016) Application of artificial neural networks for well logs. In: International petroleum technology conference. Doha, Qatar, pp 1–8. https://doi.org/10.2523/IPTC-17475-MS
Kong X, Jiang Z, Zheng Y et al (2020) Organic geochemical characteristics and organic matter enrichment of mudstones in an Eocene saline lake, Qianjiang Depression, Hubei Province, China. Mar Pet Geol 114:104194. https://doi.org/10.1016/j.marpetgeo.2019.104194
Koyi HA, Mansurbeg H (2021) The role of multiple weak lithologies in the deformation of cover units in the northwestern segment of the Zagros fold-and-thrust belt. J Pet Geol 44:145–166. https://doi.org/10.1111/jpg.12783
Lawa FA, Qader BO, Fattah AI (2020) Biostratigraphic analysis of the Oligocene-Early Miocene successions from Sulaimani area, Kurdistan Region, Iraq. Iraqi Geol J 19–41. https://doi.org/10.46717/igj.53.2D.2MS-2020-10-24
Mamaseni WJ, Naqshabandi SF, Al-Jaboury FK (2018) Petrophysical properties of the early cretaceous formations in the Shaikhan oilfield/Northern Iraq. Earth Sci Res J 22:45–52. https://doi.org/10.15446/esrj.v22n1.66088
Mohammed M, Salih H, Mnaty K (2021) Reservoir characterization of the middle cretaceous Mishrif formation in the Buzurgan oilfield, Southern Iraq. Iraqi Natl J Earth Sci 21:63–77. https://doi.org/10.33899/earth.2021.170388
Mohammed A, Dhaidan M, Al-Hazaa SH et al (2022) Reservoir characterization of the upper Turonian – lower Coniacian Khasib formation, South Iraq: Implications from electrofacies analysis and a sequence stratigraphic framework. J African Earth Sci 186:104431. https://doi.org/10.1016/j.jafrearsci.2021.104431
Morris RL, Biggs WP (1967) Using log-derived values of water saturation and porosity. SPWLA 8th Annu. Logging Symp. 26
Peters KE, Moldowan JM (1993) The biomarker guide: Interpreting molecular fossils in petroleum and ancient sediments. Prentice Hall, New Jersey
Pitman JK, Steinshouer D, Lewan M (2004) Petroleum generation and migration in the Mesopotamian Basin and Zagros fold belt of Iraq: Results from a basin-modeling study. GeoArabia 9:41–72
Powell T, McKirdy D (1973) Relationship between Ratio of Pristane to Phytane, Crude Oil Composition and Geological Environment in Australia. Nature 243:37–39. https://doi.org/10.1038/physci243037a0
Sadooni FN, Aqrawi AAM (2000) Cretaceous sequence stratigraphy and petroleum potential of the Mesopotamian Basin, Iraq. Middle East Model Jurassic/Cretaceous Carbonate Syst 69:0
Schlumberger (1972) Schlumberger log interpretation principles, 1st edn. Schlumberger Limited
Schlumberger (1989) Interpretation principles/applications. Schlumberger Educational Services
Selley RC, Sonnenberg SA (2015) Chapter 6 - the reservoir. In: Selley RC, Sonnenberg SA (eds) Elements of petroleum geology, 3rd edn. Academic Press, Boston, pp 255–320. https://doi.org/10.1016/B978-0-12-386031-6.00006-0
Singh S (2008) Permeability prediction using artificial neural network (ANN): a case study of Uinta Basin. SPE Annu Tech Conf 1–8. https://doi.org/10.2118/99286-stu
Sissakian VK, Karim SA, Al-Kubaisyi KN et al (2016) The Miocene Sequence in Iraq, a Review and Discussion, with emphasize on the Stratigraphy, Paleogeography and Economic Potential. J Earth Sci Geotech Eng 6:1792–9660
Sofer Z (1984) Stable carbon isotope compositions of crude oils: application to source depositional environments and petroleum alteration. AAPG Bull (United States) 68(1):31–49 (https://doi.org/10.1306/AD460963-16F7-11D7-8645000102C1865D)
ten Haven HL, de Leeuw JW, Rullkötter J, Damsté JSS (1987) Restricted utility of the pristane/phytane ratio as a

palaeoenvironmental indicator. Nature 330:641–643. https://doi.org/10.1038/330641a0
Thompson CL, Dembicki H (1986) Optical characteristics of amorphous kerogens and the hydrocarbon-generating potential of source rocks. Int J Coal Geol 6:229–249. https://doi.org/10.1016/0166-5162(86)90003-0
Tiab D, Donaldson EC (2004) Petrophysics: theory and practice of measuring reservoir rock and fluid transport properties, 2nd edn. Gulf Professional Publishing, New York
Tiab D, Donaldson EC (2015) Petrophysics: theory and practice of measuring reservoir rock and fluid transport properties. Gulf Professional Publishing
Timur A (1968) An Investigation Of Permeability, Porosity and Residual Water Saturation Relationships For Sandstone Reservoirs. Log Anal 9:10
Tissot B, Welte D (1984) Petroleum Formation and Occurrence, 2nd edn. Springer-Verlag, Berlin-Heidelberg-New York-Tokyo
Tucker ME, Wright VP (1990) Carbonate sedimentology. Blackwell, Oxford
Tyson RV (1993) Palynofacies Analysis. Springer Dordrecht, Dordrecht
Tyson RV (1995) Sedimentary Organic Matter: Organic Facies and Palynofacies. Springer, Netherlands
Verma AK, Cheadle BA, Routray A et al (2014) Porosity and Permeability Estimation using Neural Network Approach from Well Log Data. GeoConvention vis Conf 41276:1–6
Verma MK, Ahlbrandt TS, Al-gailani M (2004) Petroleum reserves and undiscovered resources in the total petroleum systems of Iraq: reserve growth and production implications. GeoArabia 9:51–74
Wyllie MRJ, Rose WD (1950) Some theoretical considerations related to the quantitative evaluation of the physical characteristics of reservoir rock from electrical log data. J Pet Technol 2:105–118. https://doi.org/10.2118/950105-G
Zaki B (1994) Theory, Measurement, and Interpretation of Well Logs, 6th edn. Henry L. Doherty Memorial Fund of AIME, Society of Petroleum Engineers, USA